Energy Engineering

Tech Science Press

DOI: 10.32604/ee.2024.050342

ARTICLE

Adaptive Predefined-Time Backstepping Control for Grid Connected Photovoltaic Inverter

Jiarui Zhang[1], Dan Liu[2,*], Kan Cao[2], Ping Xiong[2], Xiaotong Ji[3], Yanze Xu[1] and Yunfei Mu[1]

[1]Key Laboratory of Smart Grid of Ministry of Education, Tianjin University, Tianjin, 300072, China

[2]State Grid Hubei Electric Power Research Institute, Wuhan, 430077, China

[3]State Grid Hubei Electric Power Co., Ltd., Wuhan, 430077, China

[*]Corresponding Author: Dan Liu. Email: dannyliu66@hotmail.com

Received: 03 February 2024 Accepted: 10 April 2024 Published: 19 July 2024

ABSTRACT

The system performance of grid-connected photovoltaic (PV) has a serious impact on the grid stability. To improve the control performance and shorten the convergence time, a predefined-time controller based on backstepping technology and dynamic surface control is formulated for the inverter in the grid-connected photovoltaic. The time-varying tuning functions are introduced into state-tracking errors to realize the predefined-time control effect. To address the "computational explosion problem" in the design process of backstepping control, dynamic surface control is adopted to avoid the analytical calculations of virtual control. The disturbances of the PV system are estimated and compensated by adaptive laws. The control parameters are chosen and the global stability of the closed-loop is ensured by Lyapunov conditions. Simulation results confirm the effectiveness of the proposed controller and ensure the predefined time control in the photovoltaic inverter.

KEYWORDS

Photovoltaic inverter system; backstepping technology; predefined-time control; adaptive control

1 Introduction

As economic development accelerates, the demand for energy transformation continues to rise due to the increasing consumptions of fossil fuels [1]. In comparison to traditional fossil fuels, renewable energy offers the benefits of widespread distribution, diverse sources and reduced environmental pollution [2]. Consequently, the grid-connection rate for renewable energy is on the rise within the energy sector [3]. Furthermore, the rapid development of power electronics technology has significantly enhanced access to the deployment of renewable energy [4]. Recently, as a sustainable and clean energy source, photovoltaics has attracted more attention and investments in many countries [5–7]. Grid-connected inverters receive important research value in photovoltaic powers and renewable energy fields [8–10].

Large-scale grid-connection of photovoltaic strives for new requirements in system stability and convergence [11]. Currently, kinds of control methods have been explored in engineering practices [12–14]. In the field of microgrid control, finite-time control algorithms have been developed to track reference commands within a finite time [15–17]. In the islanded systems, the smooth power control

for PV inverters has been designed using an adaptive finite-time sliding mode technique, ensuring finite-time stability and convergence of the tracking errors [18]. Reference [19] proposes a continuous sliding mode control within finite time for grid-connected photovoltaic arrays, addressing modeling uncertainties arising from variations in converter parameters, system frequency and exogenous factors. To mitigate power chattering in the photovoltaic inverter of the master-slave island microgrid system, the adaptive sliding mode backstepping control has been studied, which can ensure the finite-time stability, favorable robustness performance and shortened convergence time of system states [20]. Finite-time control can ensure the finite time tracking of the system's solution, while the upper bound of the convergence time is influenced by the system's initial state.

Subsequently, a fixed-time control algorithm is investigated, which can ensure the convergence of tracking errors in a fixed time range. The convergence speed of fixed-time control is further enhanced and the convergence time is independent of the system's initial conditions [21]. However, the upper bound of the convergence time cannot be explicitly determined by the control parameters [21–23]. Regarding the issue of the system level frequency deviation by the power output randomness and PV generation, the control of bus overvoltage and power output is accomplished, ensuring the fixed time response in the battery energy storage systems [24]. Considering the intermittent power from renewable energy sources and frequent load fluctuations affecting the microgrid cluster, a two-layer two-level control is developed to enhance the dynamic performance of the microgrids within a fixed time [25]. Recently, deep researches on predefined time control algorithms have appeared [26,27].

Predefined time control is proposed while the upper limit of the stable time function can be determined by selecting system parameters appropriately. In [28], the secondary controller with a predefined time is formulated for the direct current (DC) microgrid, facilitating voltage regulation and current sharing among different distributed generators within a specified time. The predefined time control algorithm can provide a preset convergence time, which can be determined explicitly by the controller gains in advance [29]. The harmonics in photovoltaics have serious effects on the grid, therefore the rapid convergence of the voltage/current in photovoltaic inverters is important. Table 1 shows the comparison results of different control methods. Compared with finite time control and fixed-time control, the maximum limit of the convergence time in a predefined time control can make the theoretical value of the convergence time a simple and adjustable parameter.

Table 1: Comparison results of control methods

Control methods	Merits	Drawbacks
Backstepping finite time sliding mode control [19]	Less settling time, overshoot, oscillating response	Convergence time cannot be calculated
Fixed-time backstepping control [30]	Enhanced dynamic performance within a fixed time, regardless of initial operating values	Convergence time cannot be adjusted
Proposed control	Enhanced robustness and stability of the system, shorten convergence time within a predefined time, effective estimation of the upper limit of convergence time	Convergence time is dependent on initial states

Based on the aforementioned research, a predefined-time backstepping control is studied for the grid-connected photovoltaic inverters. The main contributions of the paper lie in:

1. A predefined time backstepping control based on initial states is proposed for the three-phase grid-connected photovoltaic inverter. The proposed control scheme ensures that the output states can convergent into a small region around the origins in a predefined time.

2. Compared to semi-global stability in [12–14], the control algorithm adopts the Lyapunov condition to ensure global closed-loop stability, realizes DC voltage tracking and unit power factor grid-connection within the predefined time.

3. In comparison with the finite-time control and fixed-time control, the proposed predefined-time control can effectively improve the convergence speed of the PV system and achieve an accurate estimation of the upper limit of convergence time.

The remainder of the paper is outlined as follows. Section 2 describes the topology architecture of the PV system, the mathematical model of the inverter and time-varying functions. Section 3 devises a predefined-time control based on backstepping and adaptive control. In Section 4, the global closed-loop stability analysis and the choices of the controller gains are present. Section 5 carries on the simulation experiments and analyses. Section 6 summarizes the paper.

2 Problem Statements

The control objective of grid-connected inverters is to maintain the stability of the DC side voltage and achieve unit power factor grid-connection. Inverters are susceptible to device aging, thermal effects, grid voltage uncertainty and external disturbances. Therefore, the control of grid-connected inverter should meet grid-connection requirements and exhibit robustness, while providing the improved system stability and convergence speed. A three-phase voltage source inverter (VSI) is modeled in a single-stage non-isolated grid-connected topology and a predefined-time control is formulated.

2.1 Dynamic Model of VSI

As shown in Fig. 1, the topology structure diagram of a three-phase photovoltaic grid-connected inverter is stated, where C_{dc} is the DC side capacitor of the inverter, u_{pv} is the output voltage of the PV array and i_{dc} is the output current. By applying Kirchhoff's voltage law, the three-phase voltage and three-phase current satisfy [31]

$$\begin{cases} L\dfrac{di_a}{dt} = -Ri_a - e_a + \dfrac{u_{dc}}{3}(2k_a - k_b - k_c) \\ L\dfrac{di_b}{dt} = -Ri_b - e_b + \dfrac{u_{dc}}{3}(-k_a + 2k_b - k_c) \\ L\dfrac{di_c}{dt} = -Ri_c - e_c + \dfrac{u_{dc}}{3}(-k_a - k_b + 2k_c) \end{cases} \tag{1}$$

Eq. (1) provides the relationship of current and voltage in the three-phase grid-connected system, where e_a, e_b, e_c are the alternating current (AC) voltages of the PV system, i_a, i_b, i_c are the AC currents of the PV system, k_a, k_b, k_c are the input switch signals, L is the inductance, R is the resistance and u_{dc} is the DC voltage of the inverter. Transforming the system (1) from the ABC coordinate into the DQ

coordinate, yields

$$\begin{cases} \dfrac{di_d}{dt} = -\dfrac{R}{L}i_d - \dfrac{e_d}{L} + \omega i_q + \dfrac{u_d}{L} \\ \dfrac{di_q}{dt} = -\dfrac{R}{L}i_q - \dfrac{e_q}{L} - \omega i_d + \dfrac{u_q}{L} \end{cases} \tag{2}$$

with $u_d = u_{dc}k_d$ and $u_q = u_{dc}k_q$, k_d and k_q are the switch signals, i_d and i_q are the grid side currents in the DQ-axis, e_d, e_q are the grid side voltages in the DQ-axis and ω is the angular frequency of the PV system.

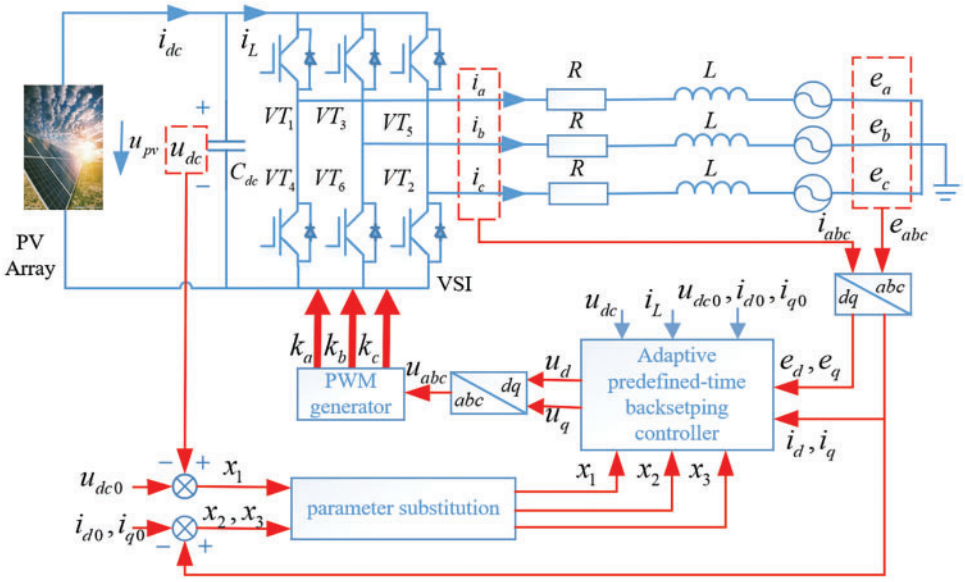

Figure 1: Topological structure diagram of three-phase PV grid-connected inverter

Basen on the Kirchhoff's current law, the voltage u_{dc} of the capacitor C_{dc} is obtained as

$$C_{dc}\frac{du_{dc}}{dt} = i_{dc} - i_L \tag{3}$$

where i_L represents the input current of VSI, i_{dc} represents the output current of the PV array, p is the active power and q is the reactive power. p and q are oriented using the vector of the grid voltage in the DQ coordinate system, $e_d = |E|$, $e_q = 0$. Here $|E|$ is the amplitude of the grid phase voltage and

$$\begin{cases} p = \dfrac{3}{2}\left(e_d i_d + e_q i_q\right) \\ q = \dfrac{3}{2}\left(e_d i_q - e_q i_d\right) \end{cases} \tag{4}$$

After ignoring the fluctuation of $|E|$, e_d is maintained as a constant, the active power p and reactive power q are proportional to the output current i_d and i_q, respectively. Therefore, ignoring the losses of VSI, the DC side voltage u_{dc} of VSI can be controlled by i_d, one has

$$i_{dc}u_{dc} = p = \frac{3e_d i_d}{2} \tag{5}$$

By invoking Eqs. (3) and (5), we can obtain

$$\frac{du_{dc}}{dt} = \frac{1}{C_{dc}}\left(\frac{3e_d i_d}{2u_{dc}} - i_L\right) \tag{6}$$

Define the reference signal of voltage u_{dc} as u_{dc0}, and the reference signal of currents i_d, i_q as i_{d0}, i_{q0}. The resulting system model for VSI is

$$\begin{cases} \dfrac{dx_1}{dt} = \dfrac{3e_d\,(x_2 + i_{d0})}{2C_{dc}\,(x_1 + u_{dc0})} - \dfrac{i_L}{C_{dc}} + d_1 \\ \dfrac{dx_2}{dt} = \dfrac{u_d}{L} - \dfrac{R}{L}\,(x_2 + i_{d0}) + \omega\,(x_3 + i_{q0}) - \dfrac{e_d}{L} + d_2 \\ \dfrac{dx_3}{dt} = \dfrac{u_q}{L} - \dfrac{R}{L}\,(x_3 + i_{q0}) - \omega\,(x_2 + i_{d0}) - \dfrac{e_q}{L} + d_3 \end{cases} \tag{7}$$

where the system state variables are chosen as $x_1 = u_{dc} - u_{dc0}$, $x_2 = i_d - i_{d0}$ and $x_3 = i_q - i_{q0}$, the control inputs are u_d and u_q. Note that d_1, d_2 and d_3 represent the unknown external disturbances of the PV system.

2.2 Preliminaries

For all headings, please capitalize the first character of each word except prepositions, and conjunctions.

The control object is to formulate the predefined time control laws u_d and u_q, then the DC voltage u_{dc} can be regulated to track the reference signal u_{dc0} at the D-axis, while the AC current i_q of the Q-axis can track the reference signal i_{q0}. Especially, the tracking errors are stable and can be ensured to remain bounded in a predefined time T_1.

Lemma 1 [32]. For an n-order system $\dot{x} = f\,(x, t, T)$ and a constant $\delta \in \mathbb{R}^+$, the solution of x is **globally predefined-time stable** if $\forall x_0 \in \mathbb{R}^n$ and $x\,(x_0, t, T) = 0_n$ hold in $t \geq T$. The solution of x satisfies **globally predefined-time boundedness** if $\forall x_0 \in \mathbb{R}^n$ and $\|x\,(x_0, t, T)\| \leq \delta$ hold when $t \geq T$. The constant parameter T represents the upper boundedness of the system stability time.

Lemma 2 [33]. For $\forall \gamma > 0$ and $e \in \mathbb{R}$, the inequality $\gamma > |e| - e \cdot sg\,(e, \gamma) \geq 0$ holds, where $sg\,(e, \gamma) = e/\sqrt{e^2 + \gamma^2}$.

The following assumptions hold for the VSI system (7).

Assumption 1 [34]. The unknown external disturbances d_1, d_2 and d_3 are bounded and continuous. That is, there exist positive constants $D_1 \in \mathbb{R}^+, D_2 \in \mathbb{R}^+, D_3 \in \mathbb{R}^+$, such that the inequalities $|d_1\,(t)| \leq D_1$, $|d_2\,(t)| \leq D_2$ and $|d_3\,(t)| \leq D_3$ hold when $t \geq 0$.

Assumption 2. The gain functions in inverter dynamics (7) are uniformly continuous satisfying $3e_d/(2C_{dc}\,(x_1 + u_{dc0})) \geq G_1 \geq 0$ and $1/L \geq G_2 \geq 0$, with $G_1, G_2 \in \mathbb{R}^+$ are known constants.

Assumption 3. Other functions in inverter dynamics (7) and their first time-derivatives are uniformly continuous.

Remark 1. Due to the randomness of photovoltaic power generation, the uncertainty of bus voltage, the aging problems and thermal effects in the inverter, disturbances terms should be considered. In practical systems, disturbances are usually subjected to various physical limitations, such as power supply stability, circuit design and the effects of filters. These factors result in the limited magnitude of disturbances within a certain range, making the disturbances bounded. Therefore, **Assumption 1**

holds. **Assumptions 2** and **3** are reasonable as active power p and reactive power q are controlled and distributed, while the grid voltage can be stabilized and considered as a constant value.

2.3 Time-Varying Function

For all headings, please capitalize the first character of each word except prepositions, and conjunctions.

The predefined time constant is introduced directly in the predefined-time control, allowing for the adjustment of different predefined times by choosing the value of the time constant in advance. The time-varying function $\rho(t)$ is adopted to achieve the predefined-time tracking of the D-axis, which satisfies the following conditions.

Condition 1. Time-varying function $\rho(t)$, the first derivative $\dot{\rho}(t)$ and the second derivative $\ddot{\rho}(t)$ are bounded on $t \geq 0$.

Condition 2. Time-varying function $\rho(t)$, the first derivative $\dot{\rho}(t)$ and the second derivative $\ddot{\rho}(t)$ are continuous on $t \geq 0$.

Condition 3. $\rho(t) = 0$ always holds when $t \geq T_1$.

Condition 4. The initial values $\rho(0)$ and $\dot{\rho}(0)$ fulfill

$$\begin{aligned} &\rho(0) = m = x_1(0) \\ &\dot{\rho}(0) = h = \frac{3e_d\left(x_2(0) + i_{d0}\right)}{2C_{dc}\left(x_1(0) + u_{dc0}\right)} - \frac{i_L}{C_{dc}} + d_1(0) \end{aligned} \tag{8}$$

where m and h are parameters related to the initial conditions, $d_1(0) = 0$ is the initial disturbance. Apparently, there are different candidates for the time-varying function $\rho(t)$. A viable option $\rho(t)$ is the quadruple polynomial form [35]

$$\rho(t) = \begin{cases} -\left(\dfrac{3m}{T_1^4} + \dfrac{h}{T_1^3}\right)t^4 + \left(\dfrac{8m}{T_1^3} + \dfrac{3h}{T_1^2}\right)t^3 - \left(\dfrac{6m}{T_1^2} + \dfrac{3h}{T_1}\right)t^2 + ht + m, & t < T_1 \\ 0, & t \geq T_1 \end{cases} \tag{9}$$

For the *1*-order system of the Q-axis, the time-varying function $\upsilon(t)$ fulfills the following conditions.

Condition 5. $\upsilon(t)$ and $\dot{\upsilon}(t)$ are bounded on $t \geq 0$.

Condition 6. $\upsilon(t)$ and $\dot{\upsilon}(t)$ are continuous on $t \geq 0$.

Condition 7. $\upsilon(t) = 0$ always holds when $t \geq T_1$.

Condition 8. The initial value $\upsilon(0)$ satisfies

$$\upsilon(0) = l = x_3(0) \tag{10}$$

and l is a parameter determined by the initial conditions.

$\upsilon(t)$ is chosen as

$$\upsilon(t) = -\begin{cases} \dfrac{3l}{T_1^4}t^4 + \dfrac{8l}{T_1^3}t^3 - \dfrac{6l}{T_1^2}t^2 + l, & t < T_1 \\ 0, & t \geq T_1 \end{cases} \tag{11}$$

Remark 2. Time-varying functions are used to achieve the desired tracking performance with a stable time-upper limit. The controller design ensures that the output tracking errors of the system

can track the desired trajectory. The upper limit of the system's convergence time can be adjusted by determining the time constant T_1 in the time-varying function.

3 Adaptive Predefined-Time Backstepping Control

The adaptive control is formulated to estimate and compensate for the disturbances in inverter model (7). The time-varying function $\rho(t)$ of the D-axis and the time-varying function $\upsilon(t)$ of the Q-axis are introduced in the definitions of the tracking errors. Based on the framework of backstepping control, the controllers u_d and u_q for the PV grid-connected inverter are designed. By presetting the upper limit of the convergence time, the closed-loop system achieves the global stability within the predefined time. For the D-axis system, a control law u_d is designed to satisfy condition $|x_1| \leq \varepsilon$ at $t \geq T_1$, where ε represents a small neighborhood of the origin. For the Q-axis, a control law u_q is designed to satisfy condition $|x_3| \leq \varepsilon$ at $t \geq T_1$.

Fig. 2 states the signal diagram of the closed-loop system. Adaptive control laws are introduced to estimate and compensate for the upper limit D_i of the external disturbances d_i $(i = 1, 2, 3)$, while the estimated values are denoted as $\widehat{D}_i$. Defining the parameter estimation errors as $\tilde{D}_i = D_i - \widehat{D}_i$. The adaptive control law is designed as

$$\dot{\widehat{D}}_i = r_i e_i sg(e_i, \gamma_i) - \sigma_i \widehat{D}_i \tag{12}$$

where $r_i > 0, \gamma_i > 0, \sigma_i > 0$ are adaptive constants.

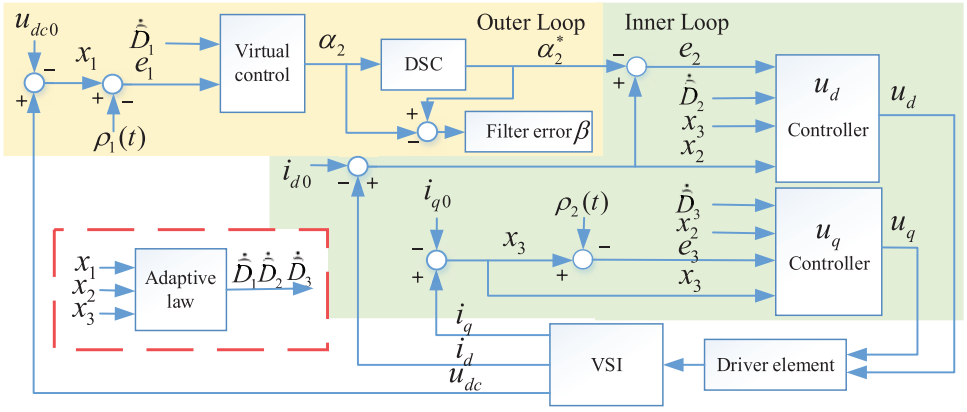

Figure 2: Signal diagram of the closed-loop system

The state tracking error is designed

$$e_1 = x_1 - \rho(t) \tag{13}$$

where $\rho(t)$ is the time-varying function of the D-axis.

The first-time derivative of e_1 is

$$\dot{e}_1 = \frac{3e_d(x_2 + i_{d0})}{2C_{dc}(x_1 + u_{dc0})} - \frac{i_L}{C_{dc}} + d_1 - \dot{\rho}(t) \tag{14}$$

The virtual control law α_2 is defined as

$$\alpha_2 = -i_{d0} + \frac{2C_{dc}(e_1 + u_{dc0})}{3e_d}\left[-k_1 e_1 + \frac{i_L}{C_{dc}} - \widehat{D}_1 sg(e_1, \gamma_1) + \dot{\rho}(t)\right] \tag{15}$$

where k_1, γ_1 are positive parameters and $sg(e_1, \gamma_1) = e_1/\sqrt{e_1^2 + \gamma_1^2}$.

Substituting the virtual controller (15) into Eq. (14) yields

$$\dot{e}_1 = -k_1 e_1 + \frac{3e_d}{2C_{dc}(x_1 + u_{dc0})}(e_2 + \beta) + d_1 - \widehat{D}_1 sg(e_1, \gamma_1) \tag{16}$$

Choose a Lyapunov function candidate V_1 as

$$V_1 = \frac{1}{2}e_1^2 + \frac{1}{2r_1}\tilde{D}_1^2 \tag{17}$$

Along the trajectories (12), (15) and (16), the first-time derivative of V_1 is

$$\begin{aligned}\dot{V}_1 &= -k_1 e_1^2 + \frac{3e_d e_1(e_2 + \beta)}{2C_{dc}(x_1 + u_{dc0})} + e_1 d_1 - e_1 \widehat{D}_1 sg(e_1, \gamma_1) - e_1 \tilde{D}_1 sg(e_1, \gamma_1) + \frac{\sigma_1}{r_1}\tilde{D}_1 \widehat{D}_1 \\ &\le -\left[k_1 - \frac{3e_d}{4C_{dc}(x_1 + u_{dc0})}\right](e_1^2 + \beta^2) + \frac{3e_d e_1 e_2}{2C_{dc}(x_1 + u_{dc0})} + \gamma_1 D_1 - \frac{\sigma_1}{2r_1}\left(\tilde{D}_1^2 - D_1^2\right)\end{aligned} \tag{18}$$

The following inequalities hold by Young's inequality

$$\begin{cases} \dfrac{3e_d e_1 \beta}{2C_{dc}(x_1 + u_{dc0})} \le \dfrac{3e_d}{4C_{dc}(x_1 + u_{dc0})}(e_1^2 + \beta^2) \\ e_1 d_1 - e_1 D_1 sg(e_1, \gamma_1) \le \gamma_1 D_1 \\ \dfrac{\sigma_1}{r_1}\tilde{D}_1 \widehat{D}_1 = \dfrac{\sigma_1}{r_1}\tilde{D}_1\left(D_1 - \tilde{D}_1\right) \le \dfrac{\sigma_1}{2r_1}\left(D_1^2 - \tilde{D}_1^2\right) \end{cases} \tag{19}$$

To avoid the "computational explosion problem" in backstepping control, the dynamic surface control (DSC) is introduced. That is, the signal α_2^* acts as the filtered signal of the virtual controller α_2^*

$$\dot{\alpha}_2^* = (\alpha_2 - \alpha_2^*)/\mu \tag{20}$$

where μ is the filter gain and $\alpha_2^*(0) = \alpha_2(0)$. Then the filtering error β is characterized as

$$\beta = \alpha_2^* - \alpha_2 \tag{21}$$

Define the state tracking errors e_2 as

$$e_2 = x_2 - \alpha_2^* \tag{22}$$

The first-time derivative of e_2 is

$$\dot{e}_2 = \frac{u_d}{L} - \frac{R}{L}(x_2 + i_{d0}) + \omega(x_3 + i_{q0}) - \frac{e_d}{L} + d_2 - \dot{\alpha}_2^* \tag{23}$$

The control laws u_d is constructed as

$$u_d = L\left[-k_2 e_2 + \frac{R}{L}(x_2 + i_{d0}) - \omega(x_3 + i_{q0}) + \frac{e_d}{L} + \dot{\alpha}_2^* - \widehat{D}_2 sg(e_2, \gamma_2) - \frac{3e_d e_1}{2C_{dc}(x_1 + u_{dc0})}\right] \tag{24}$$

where k_2 and γ_2 are the controller parameters and $sg(e_2, \gamma_2) = e_2/\sqrt{e_2^2 + \gamma_2^2}$. Substituting Eqs. (12), (20) and (24) into Eq. (23), gives

$$\dot{e}_2 = -k_2 e_2 - \frac{3e_d e_1}{2C_{dc}(x_1 + u_{dc0})} + d_2 - \widehat{D}_2 sg(e_2, \gamma_2) \tag{25}$$

Consider the following Lyapunov function V_2 as

$$V_2 = \frac{1}{2}e_2^2 + \frac{1}{2}\beta^2 + \frac{1}{2r_2}\tilde{D}_2^2 \tag{26}$$

Substituting Eq. (25) into the differential dynamic of V_2, one has

$$\begin{aligned}\dot{V}_2 &= -k_2 e_2^2 - \frac{3e_d e_1 e_2}{2C_{dc}(x_1 + u_{dc0})} - \frac{\beta^2}{\mu} - \beta\dot{\alpha}_2 + e_2 d_2 - e_2 D_2 sg(e_2, \gamma_2) + \frac{\sigma_2}{r_2}\tilde{D}_2\,\widehat{D}_2 \\ &\le -k_2 e_2^2 - \frac{3e_d e_1 e_2}{2C_{dc}(x_1 + u_{dc0})} + \gamma_2 D_2 - \left(\frac{1}{\mu} - \dot{\alpha}_2^2\right)\beta^2 + \frac{1}{4} - \frac{\sigma_2}{2r_2}\left(\tilde{D}_2^2 - D_2^2\right)\end{aligned} \tag{27}$$

with inequalities $-\beta\dot{\alpha}_2 \le \beta^2\dot{\alpha}_2^2 + 1/4$, $e_2 d_2 - e_2 D_2 sg(e_2, \gamma_2) \le \gamma_2 D_2$ and $\tilde{D}_2\,\widehat{D}_2 \le \left(D_2^2 - \tilde{D}_2^2\right)/2$ hold.

The state tracking errors e_3 of Q-axis is defined as

$$e_3 = x_3 - \upsilon(t) \tag{28}$$

where $\upsilon(t)$ is the time-varying function of the Q-axis.

The first-time derivative of e_3 is

$$\dot{e}_3 = \frac{u_q}{L} - \frac{R}{L}(x_3 + i_{q0}) - \omega(x_2 + i_{d0}) - \frac{e_q}{L} + d_3 - \dot{\upsilon}(t) \tag{29}$$

The control laws u_q is designed as

$$u_q = L\left[-k_3 e_3 + \frac{R}{L}(x_3 + i_{q0}) + \omega(x_2 + i_{d0}) + \dot{\upsilon}(t) - \widehat{D}_3 sg(e_3, \gamma_3) + \frac{e_q}{L}\right] \tag{30}$$

where k_3 and γ_3 are controller gains to be determined later, $sg(e_3, \gamma_3) = e_3/\sqrt{e_3^2 + \gamma_3^2}$. Recalling the adaptive law (12) and the *VSI* controller (30), one can get

$$\dot{e}_3 = -k_3 e_3 + d_3 - \widehat{D}_3 sg(e_3, \gamma_3) \tag{31}$$

Define a Lyapunov function candidate V_3 as

$$V_3 = \frac{1}{2}e_3^2 + \frac{1}{2r_3}\tilde{D}_3^2 \tag{32}$$

The time derivative of V_3 can be expressed as

$$\dot{V}_3 = -k_3 e_3^2 + e_3 d_3 - e_3 D_3 sg(e_3, \gamma_3) + \frac{\sigma_3}{r_3}\tilde{D}_3\,\dot{\tilde{D}}_3 \le -k_3 e_3^2 + \gamma_3 D_3 - \frac{\sigma_3}{2r_3}\left(\tilde{D}_3^2 - D_3^2\right) \tag{33}$$

where the inequalities $e_3 d_3 - e_3 D_3 sg(e_3, \gamma_3) \le \gamma_3 D_3$ and $\tilde{D}_3\,\widehat{D}_3 \le \left(D_3^2 - \tilde{D}_3^2\right)/2$ hold.

Choosing the total Lyapunov function V as

$$V = V_1 + V_2 + V_3 \tag{34}$$

From Eqs. (18), (27) and (33), $\dot{V}$ can be represented as

$$\begin{aligned}\dot{V} \le &-\left(k_1 - \frac{3e_d}{4C_{dc}(x_1 + u_{dc0})}\right)e_1^2 - k_2 e_2^2 - k_3 e_3^2 - \frac{\sigma_1}{2r_1}\tilde{D}_1^2 - \frac{\sigma_2}{2r_2}\tilde{D}_2^2 - \frac{\sigma_3}{2r_3}\tilde{D}_3^2 \\ &-\left(\frac{1}{\mu} - \frac{3e_d}{4C_{dc}(x_1 + u_{dc0})} - \dot{\alpha}_2^2\right)\beta^2 + \Gamma\end{aligned} \tag{35}$$

where $\Gamma \triangleq \gamma_1 D_1 + \gamma_2 D_2 + \gamma_3 D_3 + \frac{1}{4} + \frac{\sigma_1}{2r_1} D_1^2 + \frac{\sigma_2}{2r_2} D_2^2 + \frac{\sigma_3}{2r_3} D_3^2$.

4 Stability Analysis

By the Lyapunov theory, the predefined time stability of the closed-loop system is achieved, which is summarized in **Theorem 1**.

Theorem 1. For the inverter (7) in the PV system, the control laws u_d and u_q are proposed in (24) and (30), and the first-order filter is given by Eq. (20). For any constant $\varepsilon \in \mathbb{R}^+$, all signals in the closed-loop system can be bounded at $t \geq 0$ under the proper control gains $k_i, i = 1, 2, 3$. After the selection of control parameter T_1, $|x_1(t)| \leq \varepsilon$ and $|x_3(t)| \leq \varepsilon$ holds when $t \geq T_1$. The predefined-time stability of photovoltaic inverter is realized.

Poof. Define a vector $\zeta = \left[e_1, e_2, e_3, \beta, \tilde{D}_1, \tilde{D}_2, \tilde{D}_3\right]^T \in \mathbb{R}^7$ and a compact set Ω

$$\Omega = \left\{ \zeta \in \mathbb{R}^7 : e_1^2 + e_2^2 + e_3^2 + \beta^2 + \frac{\tilde{D}_1^2}{r_1} + \frac{\tilde{D}_2^2}{r_2} + \frac{\tilde{D}_3^2}{r_3} \leq \varepsilon^2 \right\} \tag{36}$$

The controller gains are selected as

$$\begin{cases} k_1 - \dfrac{3e_d}{4(x_1 + u_{dc0}) C_{dc}} > \dfrac{\Gamma}{\varepsilon^2}, k_2 > \dfrac{\Gamma}{\varepsilon^2}, k_3 > \dfrac{\Gamma}{\varepsilon^2} \\ \dfrac{1}{\mu} - \dfrac{3e_d}{4(x_1 + u_{dc0}) C_{dc}} - \dot{\alpha}_2^2 > \dfrac{\Gamma}{\varepsilon^2} \\ \dfrac{\sigma_1}{2} > \dfrac{\Gamma}{\varepsilon^2}, \dfrac{\sigma_2}{2} > \dfrac{\Gamma}{\varepsilon^2}, \dfrac{\sigma_3}{2} > \dfrac{\Gamma}{\varepsilon^2} \end{cases} \tag{37}$$

From Eqs. (35)–(37), we can deduce that

$$\dot{V} < -\frac{2\Gamma}{\varepsilon^2} V + \Gamma \tag{38}$$

Next, the discussion focuses on the boundedness of signals in the closed-loop system in the compact set Ω. Based on **Condition 1** and **Condition 2**, it can be inferred that $\rho(t)$, $\dot{\rho}(t)$, and $\ddot{\rho}(t)$ are consistently bounded on $t \geq 0$. From **Condition 5** and **Condition 6,** $\upsilon(t)$ and $\dot{\upsilon}(t)$ are always bounded on $t \geq 0$. While e_i and β are bounded on the set Ω.

Invoking the definition $x_1 = e_1 + \rho(t)$, as x_1 is bounded on Ω, then α_2 is bounded on the compact set Ω by virtual controller (15) and **Assumption 2**. The boundedness of x_2 can be ensured by the definition of $x_2 = e_2 + \alpha_2 + \beta$. Similarly, the boundedness of x_3 is given by $x_3 = e_3 + \upsilon(t)$. Considering the virtual controller (15), first-order filter (20) and filter error (21), the boundedness of u_d and u_q on the set Ω can be obtained from **Assumption 2** and **Assumption 3**.

The first derivation of the virtual controller α_2 can be expressed as

$$\dot{\alpha}_2 = \left(\frac{3e_d}{2C_{dc}(x_1 + u_{dc0})} \right)^{-1} \left[-k_1 \dot{e}_1 - \left(\widehat{D}_1 sg(e_1, \gamma_1) \right)' + \ddot{\rho}(t) \right] \tag{39}$$

Apparently $\dot{\alpha}_2$ is bounded on Ω from **Assumption 2**. Then, the second formula in Eq. (37) holds. An analysis is conducted on the initial states of the tracking errors. For the D-axis signal, substituting **Condition 3**, virtual controller Eq. (15) and the controller Eq. (24) into tracking errors Eqs. (13) and

(22), one has $e_1(0) = e_2(0) = 0$ on the compact set Ω. Based on $\alpha_2^*(0) = \alpha_2(0)$, $\beta(0) = 0$ holds. The Q-axis signal $e_3(0) = 0$ on the compact set Ω can be obtained. According to the controller Eqs. (24) and (39) implies that $\dot{V} < 0$ on $V = \varepsilon^2/2$. Thus, from $V(0) = 0 < \varepsilon^2/2$, $V(t) \leq \varepsilon^2/2$ always holds for $t \geq 0$.

In addition, according to Eq. (36), $|e_1(t)| \leq \varepsilon$ and $|e_3(t)| \leq \varepsilon$ holds when $t \geq 0$. Considering **Conditions 3** and **Conditions 7**, $\rho(t) = 0$ and $\upsilon(t) = 0$ hold when $t \geq T_1$. Eqs. (13) and (28) implied that $|x_1(t)| \leq \varepsilon$ and $|x_3(t)| \leq \varepsilon$ holds when $t \geq T_1$. Therefore, the solution of the PV system (7) is global predefined-time bounded according to **Lemma 1.** □

Remark 3. For $i = 1, 2, 3$, the detailed design process of the proposed control scheme is

1. Based on the initial states (8) and (10), select the suitable time-varying functions (9) and (11) to fulfill the predefined time stability conditions.

2. Choose the appropriate parameters μ and determine the first-order filter (20).

3. Choose appropriate parameters k_i, r_i, σ_i, γ_i to determine the adaptive laws (12), virtual control law (15), controllers (24) and (30).

5 Simulations

The simulation is carried on the photovoltaic system to demonstrate the effectiveness of the proposed control method. The physical parameters are as follows: $C_{dc} = 4.4\,mF$, $R = 0.5\,\Omega$, $L = 2.5\,mH$, $i_L = 50\,A$, $e_d = 270\,V$, $e_q = 0\,V$, $f = 50\,Hz$, $\omega = 314\,rad/s$, $u_{dc0} = 500\,V$, $i_{q0} = 0\,A$. Choose the controller gains as $k_1 = 120$, $k_2 = 150$ and $k_3 = 200$; The filter gain for DSC is selected as $\mu = 0.001$. Set the adaptive gains to $r_1 = 2$, $r_2 = r_3 = 5$, $\sigma_1 = 0.8$, $\sigma_2 = \sigma_3 = 0.6$, $\gamma_1 = \gamma_2 = \gamma_3 = 0.1$.

Case1. Simulations under different predefined times $T_1 = 0.1\,s$, $T_1 = 0.08\,s$, $T_1 = 0.15\,s$

The initial condition is set to $x_1(0) = -8V$, $x_2 = -2A$, $x_3(0) = 2A$. The disturbances $d_1 = 4.4$, $d_2 = 5$, $d_3 = 5$ are added between 0.2 and 0.4 s.

Fig. 3 shows the trajectories of state x_1, x_2 and x_3 when the predefined time is set to $T_1 = 0.1\,s$. From Fig. 3, the system state variables can convergent to the small neighborhood of the origin within $T_1 = 0.1\,s$. That is, the proposed predefined time backstepping control method has completed DC voltage tracking and unit power factor grid connection within the specified time, while the predefined time control goal is achieved.

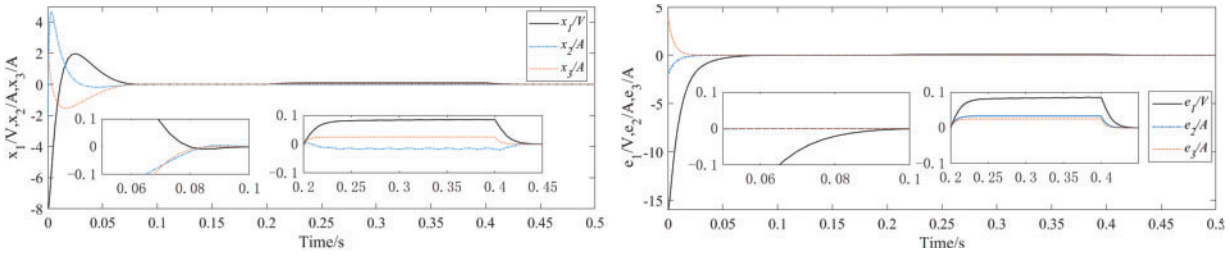

(a) state variables (b) tracking errors

Figure 3: State variables and tracking errors at $T_1 = 0.1\,s$

Figs. 4a and 5a show the trajectories of state variables x_1, x_2 and x_3 at different predefined times of $T_1 = 0.08\,s$ and $T_1 = 0.15\,s$, respectively. Figs. 4b and 5b show the trajectories of tracking errors e_1, e_2 and e_3. When the preset convergence times changes, the proposed predefined time backstepping

control method still completes *DC* voltage tracking and unit power factor grid connection within the preset time.

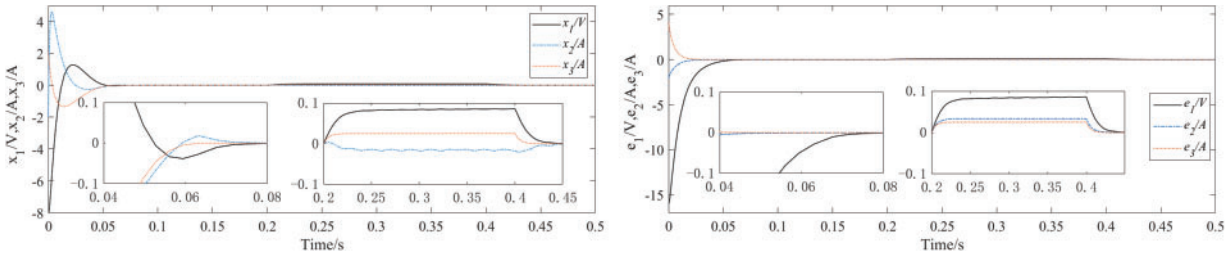

(a) state variables (b) tracking errors

Figure 4: State variables and tracking errors at $T_1 = 0.08\,s$

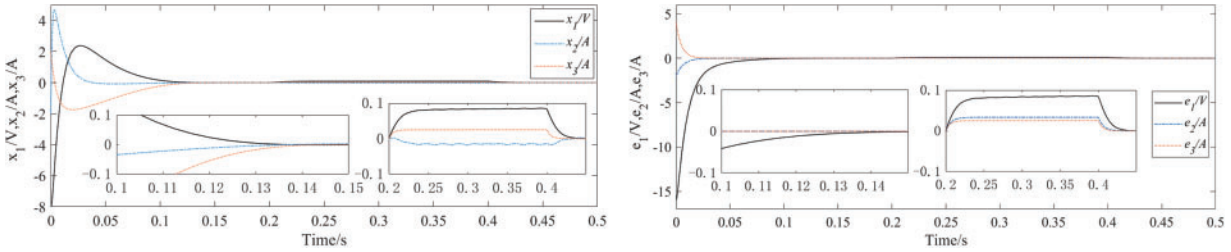

(a) state variables (b) tracking errors

Figure 5: State variables and tracking errors at $T_1 = 0.15\,s$

A comparison simulation of finite-time backstepping control and fixed-time backstepping control are performed. Fig. 6a shows the trajectories of state variables x_1, x_2, x_3 and tracking error e_2 in finite-time control, while Fig. 6b shows the trajectories of state variables x_1, x_2, x_3 and tracking error z_2 in the fixed-time control. The finite-time control can achieve the tracking in 0.35 s, while the convergence time in fixed-time control is 0.2 s. Compared with finite-time and fixed-time, the predefined time control can customize the upper limit of convergence time within the range supported by physical parameters. The proposed predefined time backstepping control can improve the convergence speed of PV systems, achieve predefined time control objectives and provide a satisfactory control performance. After disturbances are triggered, the robust performance is effectively improved.

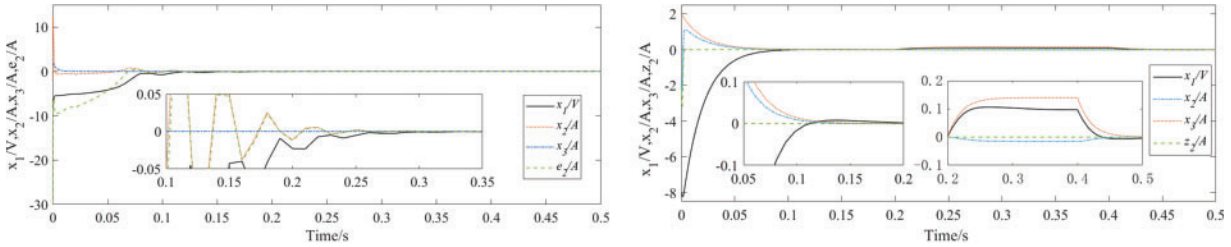

(a) finite-time backstepping control (b) fixed-time backstepping control

Figure 6: State variables and tracking errors in traditional backstepping controller

Fig. 7 shows the estimation value of the virtual control at $T_1 = 0.1\,s$. Fig. 8 shows the curves of controllers u_d and u_q under different predefined times. Although the preset time value changes, the controller achieves stable control within the different predefined time.

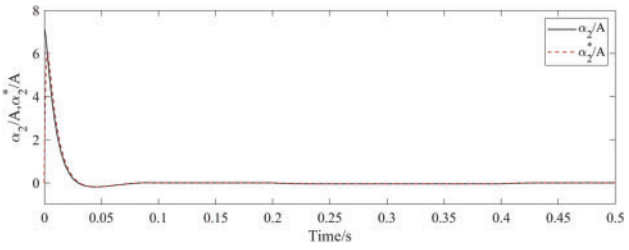

Figure 7: Estimation value of virtual controller at $T_1 = 0.1\,s$

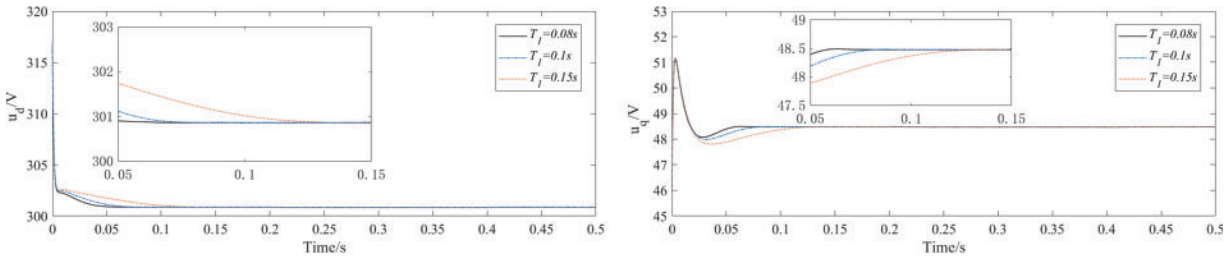

(a) control input u_q (b) control input u_q

Figure 8: Controllers under different predefined times

Case2. Simulation under different initial states

To address the tracking performance of the controller, different initial states $(4V, 3A, -1A)$, $(-5V, -3A, 6A)$ and $(10V, 6A, -5A)$ are considered.

Fig. 9 displays the state responses x_1, x_2 and x_3 under different initial states, while Fig. 10 illustrates the tracking errors e_1, e_2 and e_3 under different initial states, set the predefined time to 0.1 s. The control can achieve effective tracking within the predefined time under the different initial values.

Fig. 11 illustrates the curves of state variables in finite time backstepping control under different initial states. Apparently, the tracking process of state variables is slow and the trajectory changes are small under different initial states, achieving tracking about 0.35 s. Fig. 12 depicts the state responses variables in a fixed-time controller under different initial states. The convergence time of fixed time control has been improved and effective tracking can be achieved in different initial states, while the tracking goal is reached within 0.2 s. Compared with finite-time control and fixed-time control, predefined time control can approach the upper limit of convergence time more accurately, while provide the improved convergence speed and control performance effectively.

Figs. 13–15 show the controllers' trajectories in finite-time control, fixed-time control, and predefined-time control, respectively. Based on the simulation results, the predefined-time backstepping controllers and can achieve grid-connection objectives within the predefined time, effectively reduce the convergence time and improve the quality of grid-connected electrical energy.

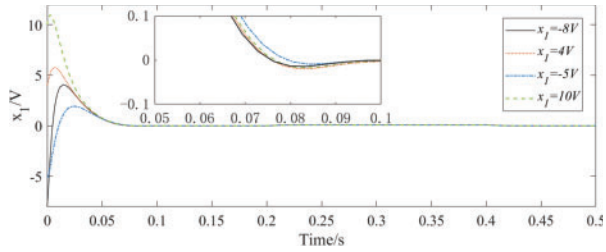

(a) the state response x_1

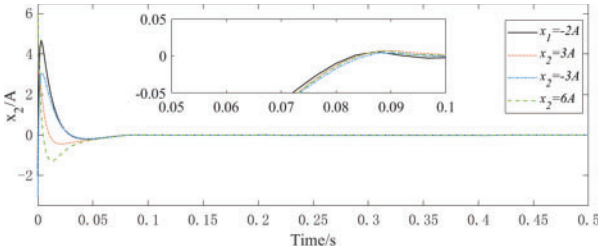

(b) the state response x_2

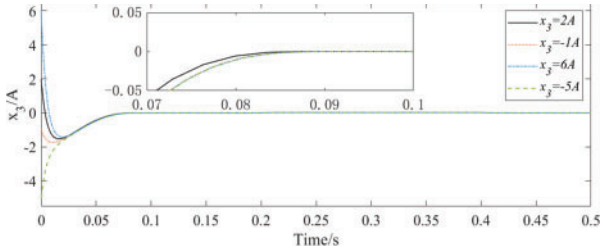

(c) the state response x_3

Figure 9: State response under different initial states at $T_1 = 0.1\,s$

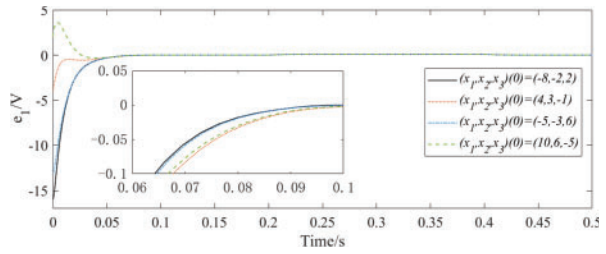

(a) tracking error e_1

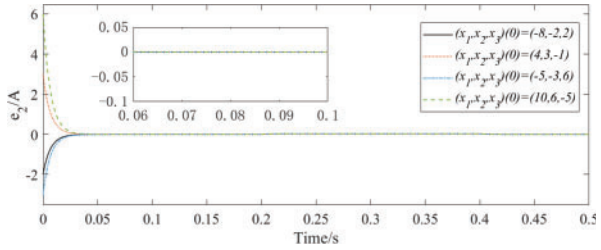

(b) tracking error e_2

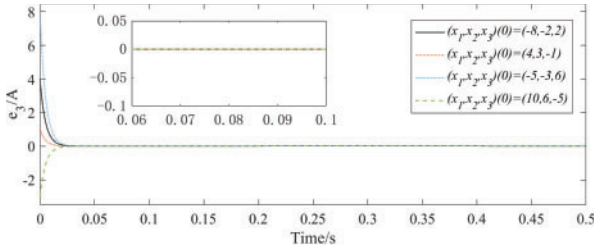

(c) tracking error e_3

Figure 10: Tracking errors under different initial states at $T_1 = 0.1\,s$

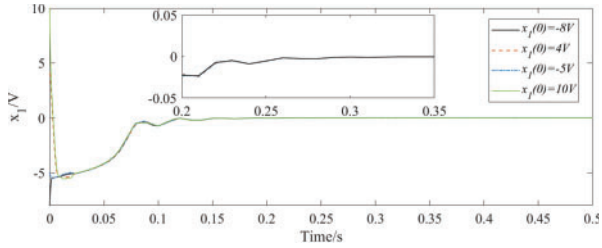

(a) the state response x_1

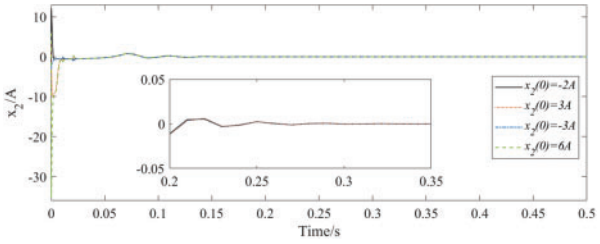

(b) the state response x_2

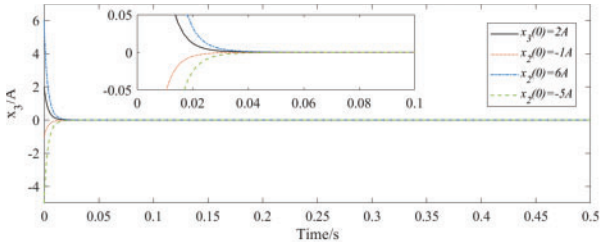

(c) the state response x_3

Figure 11: State responses under different initial states in finite-time backstepping controller

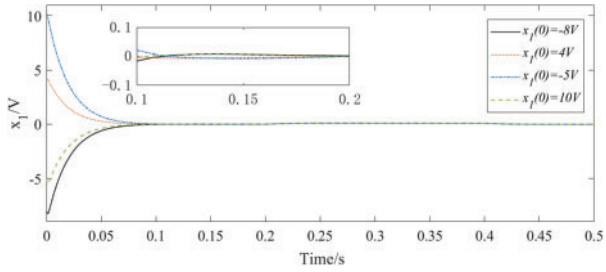

(a) the state response x_1

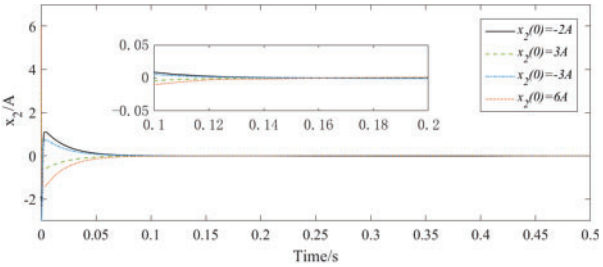

(b) the state response x_2

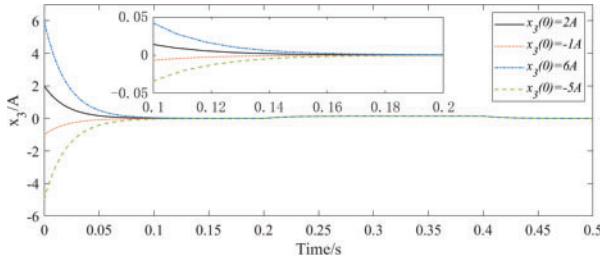

(c) the state response x_3

Figure 12: State responses under different initial states in fixed-time backstepping controller

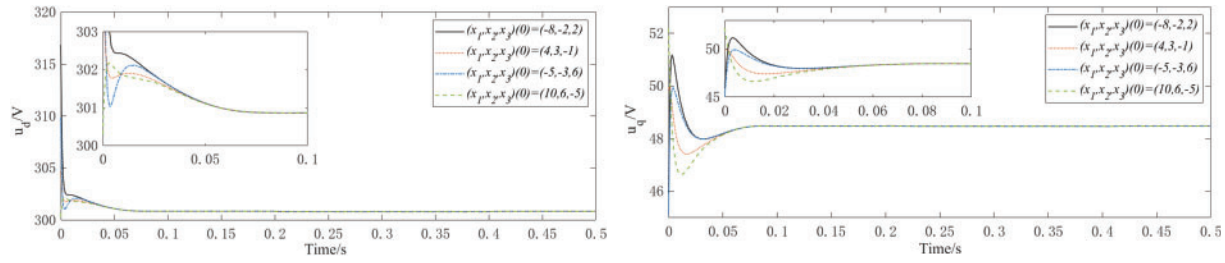

(a) input control u_d (b) input control u_d

Figure 13: Controllers under different initial states at $T_1 = 0.1\,s$

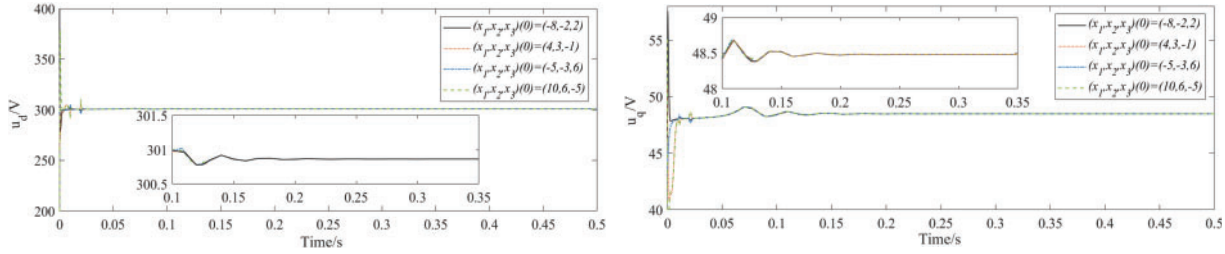

(a) input control u_d (b) input control u_d

Figure 14: Controllers under different initial states in finite-time backstepping controller

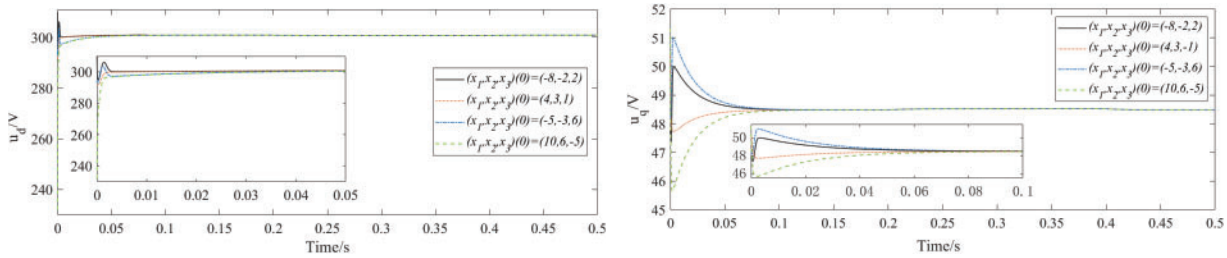

(a) input control u_d (b) input control u_d

Figure 15: Controllers under different initial states in fixed-time backstepping controller

6 Conclusion

To realize the effective control of *VSI* in a grid-connected *PV* system, a predefined-time controller is formulated. The time-varying functions are introduced in state tracking errors during the backstepping recursive design. Analytical differential calculation of the virtual control in backstepping control is avoided by the *DSC* strategy, and the disturbance compensation is realized by adaptive control. Furthermore, the global stability of the proposed predefined time control is verified by the Lyapunov theory. The simulation results demonstrate that the proposed predefined-time controller can implement predefined-time control and has excellent control performance for the inverter. The predefined time control method proposed in this paper can track the DC voltage and connect the unit power factor to the grid in the predefined time, but it depends on the initial states of the system, which should be solved in the future research.

Acknowledgement: Thanks to the editors and the anonymous reviewers for the helpful comments and suggestions that improve the presentation of the manuscript.

Funding Statement: This work was supported by the State Grid Corporation of China Headquarters Science and Technology Project under Grant No. 5400-202122573A-0-5-SF.

Author Contributions: The authors confirm contribution to the paper as follows: Dan Liu and Yanze Xu contributed to controller formulation. Kan Cao and Ping Xiong contributed to system stability analysis. Jiarui Zhang and Yunfei Mu wrote the manuscript and performed the simulations experiment. Xiaotong Ji contributed to the conception of the paper significantly. All authors reviewed the results and approved the final version of the manuscript.

Availability of Data and Materials: The authors confirm that the data supporting the findings of this study are available within the article. Additional data that support the findings of this study are available upon request from the corresponding author, subject to reasonable request.

Conflicts of Interest: The authors declare that they have no conflicts of interest to report regarding the present study.

References

1. J. Chen, Y. Lv, and T. Fan, "Research on the evolution and driving factors of digitalization of energy in China–A new perspective based on coupling coordination," *Heliyon*, vol. 9, no. 3, May 2023. doi: 10.1016/j.heliyon.2023.e14138.
2. D. Pullaguram, S. Mishra, and N. Senroy, "Event-triggered communication based distributed control scheme for DC microgrid," *IEEE Trans. Power Syst.*, vol. 33, no. 5, pp. 5583–5593, Sep. 2018. doi: 10.1109/TPWRS.2018.2799618.
3. R. H. Lasseter, Z. Chen, and D. Pattabiraman, "Grid-forming inverters: A critical asset for the power grid," *IEEE J. Emerg. Sel. Top. Power Electron.*, vol. 8, no. 2, pp. 925–935, Dec. 2019. doi: 10.1109/JESTPE.2019.2959271.
4. Y. X. Ji, W. He, S. J. Cheng, K. Jürgen, and M. Zhan, "Dynamic network characteristics of power-electronics-based power systems," *Sci. Rep.*, vol. 10, no. 1, pp. 9946, Jun. 2020. doi: 10.1038/s41598-020-66635-0.
5. L. Zhang, Z. Chen, H. Zhang, Z. H. Ma, B. W. Cao and L. H. Song, "Accurate study and evaluation of small PV power generation system based on specific geographical location," *Energy Eng.*, vol. 117, no. 6, pp. 453–470, Aug. 2020. doi: 10.32604/EE.2020.013276.
6. H. Abubakr, J. C. Vasquez, K. Mahmoud, M. M. F. Darwish, and J. M. Guerrero, "Comprehensive review on renewable energy sources in Egypt-current status, grid codes and future vision," *IEEE Access*, vol. 10, pp. 4081–4101, Mar. 2022. doi: 10.1109/ACCESS.2022.3140385.
7. F. Hasan, J. H. Ahmed, and N. K. Abdul Hadi, "Performance analysis of a rooftop hybrid connected solar PV system," *Energy Eng.*, vol. 119, no. 4, pp. 1729–1744, 2022. doi: 10.32604/ee.2022.021190.
8. M. Inci, "Technoeconomic analysis of fuel cell vehicle-to-grid (FCV2G) system supported by photovoltaic energy," *Energy Technol.*, vol. 11, no. 4, pp. 2201162, Apr. 2023. doi: 10.1002/ente.202201162.
9. M. İnci and K. Ç. Bayındır, "Single-stage vehicular fuel cell system with harmonic elimination capability to suppress distortion effects of electric vehicle parking lots," *J. Power Sources*, vol. 597, pp. 234175, Mar. 2024. doi: 10.1016/j.jpowsour.2024.234175.
10. M. İnci, "Connecting multiple vehicular PEM fuel cells to electrical power grid as alternative energy sources: A case study," *Int. J. Hydrogen Energy*, vol. 52, pp. 1035–1051, Jan. 2024. doi: 10.1016/j.ijhydene.2023.08.228.

11. X. Deng, F. P. Da, H. J. Shao, and X. Wang, "A survey of the researches on grid-connected solar power generation systems and power forecasting methods based on ground-based cloud atlas," *Energy Eng.*, vol. 120, no. 2, pp. 385–408, Jul. 2023. doi: 10.32604/ee.2023.023480.
12. D. Z. Xu, Y. C. Dai, C. S. Yang, and X. G. Yan, "Adaptive fuzzy sliding mode command-filtered backstepping control for islanded PV microgrid with energy storage system," *J. Frank. Inst. Eng. Appl. Math.*, vol. 356, no. 4, pp. 1880–1898, Mar. 2019. doi: 10.1016/j.jfranklin.2019.01.012.
13. X. Shi, Y. Cheng, C. Yin, X. Huang, and S. M. Zhong, "Design of adaptive backstepping dynamic surface control method with RBF neural network for uncertain nonlinear system," *Neurocomputing*, vol. 330, pp. 490–503, Feb. 2019. doi: 10.1016/j.neucom.2018.11.029.
14. S. Dhar and P. K. Dash, "Adaptive backstepping sliding mode control of a grid interactive PV-VSC system with LCL filter," *Sustain. Energy, Grids Netw.*, vol. 6, pp. 109–124, Jun. 2016. doi: 10.1016/j.segan.2016.03.001.
15. Z. X. Zhong, X. Y. Wang, and H. K. Lam, "Finite-time fuzzy sliding mode control for nonlinear descriptor systems," *IEEE/CAA J. Autom. Sin.*, vol. 8, no. 6, pp. 1141–1152, Jun. 2021. doi: 10.1109/JAS.2021.1004024.
16. El. J. Khazane and E. H. Tissir, "Achievement of MPPT by finite time convergence sliding mode control for photovoltaic pumping system," *Sol. Energy*, vol. 166, pp. 13–20, May 2018. doi: 10.1016/j.solener.2018.03.026.
17. M. Y. Xie, M. M. Gulzar, H. Tehreem, M. Y. Javed, and S. T. H. Rizvi, "Automatic voltage regulation of grid connected photovoltaic system using Lyapunov based sliding mode controller: A finite-time approach," *Int. J. Control Autom. Syst.*, vol. 18, pp. 1550–1560, Jun. 2020. doi: 10.1007/s12555-019-0563-x.
18. P. Zhang, G. R. Zhang, and H. B. Du, "Finite-time consensus for power regulation of parallel PV Grid-connected inverters," *IEEE Trans. Circuits Syst. II-Express Briefs*, vol. 67, no. 11, pp. 2632–2636, Nov. 2020. doi: 10.1109/TCSII.2020.2964956.
19. S. Dhar and P. K. Dash, "A new backstepping finite time sliding mode control of grid connected PV system using multivariable dynamic VSC model," *Int. J. Electr. Power& Energy Syst.*, vol. 82, pp. 314–330, Nov. 2016. doi: 10.1016/j.ijepes.2016.03.034.
20. C. S. Yang, S. F. Ni, Y. C. Dai, X. N. Huang, and D. D. Zhang, "Anti-disturbance finite-time adaptive sliding mode backstepping control for PV inverter in master-slave-organized islanded microgrid," *Energies*, vol. 13, no. 17, pp. 4490, Sep. 2020. doi: 10.3390/en13174490.
21. W. Y. Jiang, S. S. Ge, and D. Y. Li, "Fixed-time-synchronized control: A system-dimension-categorized approach," *Sci. China Inf. Sci.*, vol. 66, no. 7, pp. 1–18, Jul. 2023. doi: 10.1007/s11432-022-3649-1.
22. L. N. Liu and G. H. Yang, "Distributed fixed-time optimal resource management for microgrids," *IEEE Trans. Autom. Sci. Eng.*, vol. 20, no. 1, pp. 404–412, Jan. 2022. doi: 10.1109/TASE.2022.3155163.
23. S. Shi, G. S. Zhang, H. F. Min, Y. L. Hu, and Y. H. Sun, "Exact uncertainty compensation of linear systems by continuous fixed-time output-feedback controller," *J. Syst. Eng. Electron.*, vol. 33, no. 3, pp. 706–715, Jun. 2022. doi: 10.23919/JSEE.2022.000065.
24. L. Y. Xiong *et al.*, "Voltage and frequency regulation with WT-PV-BESS in remote weak grids via fixed-time containment control," *IEEE Trans. Power Syst.*, vol. 38, pp. 2719–2735, May 2023. doi: 10.1109/TPWRS.2022.3190847.
25. S. Sahoo, S. Mishra, S. Fazeli, F. R. Li, and T. Dragicevic, "A distributed fixed-time secondary controller for DC microgrid clusters," *IEEE Trans. Energy Convers.*, vol. 34, no. 4, pp. 1997–2007, Dec. 2019. doi: 10.1109/TEC.2019.2934905.
26. Y. N. Pan, W. Y. Ji, and H. J. Liang, "Adaptive predefined-time control for Lü chaotic systems via backstepping approach," *IEEE Trans. Circuits Syst. II: Express Briefs*, vol. 69, no. 12, pp. 5064–5068, Dec. 2022. doi: 10.1109/TCSII.2022.3204050.
27. R. E. Jiménez, T. J. D. Sánchez, G. D. Gómez, and A. G. Loukinanov, "Variable structure predefined-time stabilization of second-order systems," *Asian J. Control*, vol. 21, no. 3, pp. 1179–1188, May 2019. doi: 10.1002/asjc.1785.

28. Y. Zhang, Y. W. Wang, J. W. Xiao, and X. K. Liu, "Predefined-time secondary control for DC microgrid," *IEEE Trans. Ind. Electron.*, vol. 69, no. 12, pp. 13504–13513, Dec. 2021. doi: 10.1109/TIE.2021.3128899.
29. F. L. Jia, J. Huang, and X. He, "Adaptive predefined-time tracking control for high-order strict-feedback nonlinear systems with unknown mismatched disturbances," *Int. J. Adapt Control Signal Process*, vol. 36, no. 11, pp. 2903–2919, Sep. 2022. doi: 10.1002/acs.3502.
30. J. A. Moreno, "Arbitrary-order fixed-time differentiator," *IEEE Trans. Automat. Contr.*, vol. 67, no. 3, pp. 1543–1549, May 2022. doi: 10.1109/TAC.2021.3071027.
31. D. Xu, G. Wang, W. Yan, and C. Shen, "Nonlinear adaptive command-filtered backstepping controller design for three-phase grid-connected solar photovoltaic with unknown parameters," presented at the 2017 Chinese Autom. Congr., Jinan, China, Oct. 20–22, 2017, pp. 7823–7827.
32. R. E. Jiménez, V. A. Muñoz, T. J. D. Sánchez, M. Defoort, and A. G. Loukianov, "A Lyapunov-like characterization of predefined-time stability," *IEEE Trans. Automat. Contr.*, vol. 65, no. 11, pp. 4922–4927, Nov. 2020. doi: 10.1109/TAC.2020.2967555.
33. C. Song, H. B. Sun, and L. L. Hou, "A predefined time decentralized adaptive tracking control method for interconnected nonlinear systems," *Int. J. Robust Nonlinear Control*, vol. 33, no. 13, pp. 7986–8014, Sep. 2023. doi: 10.1002/rnc.6806.
34. H. Bécerra, C. Vázquez, G. Arechavaleta, and J. Delfin, "Predefined-time convergence control for high-order integrator systems using time base generators," *IEEE Trans. Control Syst. Technol.*, vol. 26, no. 5, pp. 1866–1873, Sep. 2018. doi: 10.1109/TCST.2017.2734050.
35. B. J. Liu, M. S. Hou, C. H. Wu, W. C. Wang, Z. H. Wu and B. Huang, "Predefined-time backstepping control for a nonlinear strict-feedback system," *Int. J. Robust Nonlinear Control*, vol. 31, no. 8, pp. 3354–3372, Feb. 2021. doi: 10.1002/rnc.5425.